Astronomy & Astrophysics manuscript no. output
September 9, 2019

MCDHF and RCI calculations of energy levels, lifetimes, and transition rates in Si III and Si IV⋆

B. Atalay[1,2], T. Brage[1,4], P. Jönsson[3], and H. Hartman[3]

[1] Department of Physics, Lund University, Post Office Box 118, SE-22100 Lund, Sweden
e-mail: betul.atalay@teorfys.lu.se, batalay@comu.edu.tr
[2] Department of Physics, Çanakkale Onsekiz Mart University, Çanakkale, Turkey
[3] Materials Science and Applied Mathematics, Malmö University, SE-20506 Malmö, Sweden
[4] Institute of Modern Physics, Fudan University, Shanghai, PRC

Received-, 2018;

ABSTRACT

We present extensive multiconfiguration Dirac-Hartree-Fock and relativistic configuration interaction calculations including 106 states in doubly ionized silicon (Si III) and 45 states in triply ionized silicon (Si IV), which are important for astrophysical determination of plasma properties in different objects. These calculations represents an important extension and improvement of earlier calculations especially for Si III. The calculations are in good agreement with available experiments for excitation energies, transition properties, and lifetimes. Important deviations from the NIST-database for a selection of perturbed Rydberg series are discussed in detail.

Key words. Atomic data, Silicon, Na-like ions, Mg-like ions

1. Introduction

Silicon is one of the most abundant elements on Earth and in the Universe. Due to its high abundance, the lowest ionization ions of Silicon, Si I-IV, play important roles in the diagnostics and modeling of various astrophysical (Becker & Butler 1990; Catanzaro et al. 2008; Iijima & Nakanishi 2008) and laboratory plasmas (Cowpe et al. 2008; Yamazaki et al. 2009; Ogilvie & Nicolich 2009). Si I and Si II have been extensively studied both experimentally and theoretically, see for example Pehlivan Rhodin (2018) and references given therein.

Lines from Si III and Si IV are observed in the spectra of several different astronomical objects, for example the solar corona and transition region, early-type stars, planetary nebulae, novae, and the interstellar medium, where they have been used for diagnostics of the plasma parameters (Dufton et al. 1983; Nussbaumer 1986; Rubin et al. 1993). As an example, Dufton et al. (1983) used the Si III emission lines observed by Skylab to determine the electron density of the solar corona. Discrepancies between observed and predicted Si III line ratios involving the intercombination line $3s^2\ ^1S_0$ - $3s3p\ ^3P_1$ at 1892 Å and the higher excitation $3s3p\ ^1P_1$ - $3s4s\ ^1S_0$ at 1313 Å were found. The authors suggested it may have been caused by the presence of a non-Maxwellian electron distributions changing the intensity ratio between the lines. The energy of the upper level of the 1313 Å line is considerably higher than the average electron thermal energy, and the excitation from the ground state can be increased by high-energy electrons (Pinfield et al. (1999). Similarly, Keenan et al. (1989) presented Spacelab 2 observations and Pinfield et al. (1999) presented spectra from the Solar Ultraviolet Measurements of Emitted Radiation (SUMER) instrument onboard the Solar and Heliospheric Observatory (SOHO) to give a deeper analysis of possible non-Maxwellian emission-line enhancement in different solar regions. The suggestion of the presence of non-Maxwellian electron distributions was followed up by Dzifčáková & Kulinová (2011). More recently, Del Zanna et al. (2015) investigated the main spectral diagnostics for Si III ultraviolet lines, to measure electron densities and temperatures. However, they found no conclusive evidence for the presence of non-Maxwellian electron distributions from observations of the low transition region of the solar atmosphere, based on *R*-matrix scattering calculations for electron collisional excitation of Si III, carried out with the intermediate-coupling frame transformation method. The updated and more accurate atomic data of Si III in the present paper, can be used for rederivation of the plasma diagnostics using existing solar observations.

Due to their relatively high ionization energies, lines from Si III and Si IV appear in early-type stars, for example B-type stars, which are massive stars with surface temperatures 10 000–30 000 K showing strong Si III and Si IV lines in their optical spectra. The present-day chemical abundances of the Galaxy in the solar vicinity, can be determined by studying B-type main sequence stars due to their short lifetimes (Przybilla et al. 2008; Simón-Díaz, S. 2010). The silicon ionization balance is used as the temperature diagnostics in the B-type star temperature range. Becker & Butler (1990) used Si III and Si IV spectral lines to determine the temperature, whereas Monteverde et al. (2000) studied the ionization equilibria of Si III compared to Si II and Si IV, respectively, to find the Si-abundance. A recent study by Nieva & Przybilla (2012) analyzed 29 early B-type stars in OB associations with a thorough and self-consistent analysis technique. They found the present-day Solar neighborhood to be chemically homogeneous, indicating abundance fluctuations of

⋆ Tables 1 and 2 are only available in electronic form at the CDS via anonymous ftp to cdsarc.u-strasbg.fr (130.79.128.5)or via http://cdsweb.u-strasbg.fr/cgi-bin/qcat?J/A+A/

Article published by EDP Sciences, to be cited as https://doi.org/10.1051/0004-6361/201935618

less than 10 % around the mean. Bailey & Landstreet (2013) carried out a study on the determination of the abundance of Si to clarify discordant results in mid to late B-type stars.

The atomic data parameters, particularly transition rates, are essential in the abundance determination and plasma modeling. The work presented here therefore aims to provide accurate atomic data for a large part of the Si III and Si IV spectrum.

2. Previous work on atomic data for Si III and Si IV

Berry et al. (1971) and Livingston et al. (1976a,b) performed radiative lifetime measurements in Si III and Si IV using the beam-foil technique. Kwong et al. (1983) used a radio-frequency ion trap to measure the lifetime of the long-lived $3s3p\ ^3P_1^o$ level of Si III by observation of the decay to the ground state at 1892 Å and obtained an A-value of $(1.67 \pm 0.1) \times 10^4$ s^{-1}. This result has been included in many later plasma models. Later studies, for instance Ojha et al. (1988), confirm this value.

On the theoretical side, Nussbaumer (1986) used a multiconfiguration approach with an adjustable Thomas-Fermi potential to determine the transition probabilities for the 17 lowest terms in Si III. They applied various semi-empirical corrections based on the observed energies to improve the accuracy in the term energies. Butler et al. (1993) computed the radiative data for the $3l3l'$ transitions, for Si III and other Mg-like ions of astrophysical interests by using the close-coupling approximation with a modified version of the R-Matrix code as a part of the international Opacity project (Seaton 1987). Safronova et al. (2000) used relativistic second-order many body perturbation theory (MBPT) to calculate excitation energies and transition rates for the same transition arrays. Almaraz et al. (2000) applied the CIV3 code (Hibbert 1975) to calculate energy levels and oscillator strengths in Si III.

In more recent studies, Del Zanna et al. (2015) performed a large-scale R-matrix scattering calculation providing 149 LS terms and 283 fine-structure levels arising from 3snl, 3pnl and 3dnl configurations with $n \leq 5$ and $l \leq 4$. Aggarwal (2017) reported energies and lifetimes for the 141 levels of the $3l3l'$ and $3l4l'$ configurations and radiative rates for four types of transitions (E1, E2, M1, and M2) in Si III. Iorga & Stancalie (2018) investigated the effect of core-valence and core-core correlations on the energy levels and transition probabilities in the Mg isoelectronic sequence using the Flexible Atomic Code (FAC) (Gu 2008). The results contained the energy of the levels arising from the valence configurations along with transition rates corresponding to E1, M1, E2, M2 transitions between states arising from $3l3l'$ with $l, l' \leq 2$ and $3snl''$ with $n \leq 7$ and $l'' \leq 4$ configurations.

Froese Fischer et al. (2006) performed extensive and highly accurate multiconfiguration Hartree-Fock (MCHF) calculations for the Mg-like sequences ($Z = 12, ..., 26$). They used Breit-Pauli approximation to include relativistic effects. They computed both allowed (E1) and some forbidden (E2, M1, M2) transitions.

For triply ionized silicon Maniak et al. (1993) performed radiative lifetime measurements of $3p, 3d$, and $4s$ levels using the beam-foil technique. Theodosiou & Curtis (1988) used a semi-empirical quantum defect approach to calculate lifetimes for the $3p\ ^2P_{1/2}$, $3p\ ^2P_{3/2}$, $3d\ ^2D_{3/2}$, and $3d\ ^2D_{5/2}$ levels in the Na isoelectronic sequence. These calculations reached a fair agreement with experiments, but deviated from some ab initio results. Siegel et al. (1998) used a semi-empirical model potential approach to compute electric dipole transition oscillator strengths for low-lying transitions in the Na isoelectronic sequence (Na I - Ca X). The core polarization effects were explicitly included in the calculations. Siems et al. (2001) presented oscillator strengths and lifetimes for Si IV using a multiconfiguration Hartree-Fock relativistic (HFR) approach. In recent years, Nandy & Sahoo (2015) carried out calculations of the relativistic sensitivity coefficients, oscillator strengths, transition probabilities, lifetimes, and magnetic dipole hyperfine structure constants for a number of low-lying states in the Zn II, Si IV, and Ti IV. Safronova et al. (1998) carried out all-order relativistic many-body calculations of removal energies and hyperfine constants for $3s, 3p_{1/2}, 3p_{3/2}, 3d_{3/2}, 3d_{5/2}$, and $4s$ states of Na-like ions with $Z = 11 - 16$. The reduced dipole matrix elements were determined for $3p_{1/2} - 3s$, $3p_{3/2} - 3s$, $4s - 3p_{1/2}$, $4s - 3p_{3/2}$, $3d_{3/2} - 3p_{1/2}$, $3d_{3/2} - 3p_{3/2}$, and $3d_{5/2} - 3p_{3/2}$ electric-dipole transitions. The calculations included single and double excitations of the Hartree-Fock ground state to all orders in perturbation theory. Theoretical fine-structure intervals had an agreement with measurements to about 0.3% for $3p$ states and to about 3% for $3d$ states. Theoretical hyperfine constants and line strengths agreed with the precise measurements to better than 0.3%. Finally, Froese Fischer et al. (2006) performed extensive ab initio non-orthogonal spline CI calculations for the Na-like sequence. Kelleher & Podobedova (2008) presented the latest compilation of Si III and Si IV transition rates.

3. Theory

In this work, the calculations were performed using the fully relativistic multi-configuration Dirac-Hartree-Fock (MCDHF) method in jj-coupling (Grant 2007; Froese Fischer et al. 2016).

3.1. Multiconfiguration Dirac-Hartree-Fock

An electronic state of a many electrons system is determined by a wave function Ψ, which is a solution to the wave equation:

$$H\Psi = E\Psi, \tag{1}$$

where H is the Hamiltonian operator and E is the total energy of the system. The common starting point of the MCDHF method is the Dirac-Coulomb Hamiltonian:

$$H_{DC} = \sum_{i=1}^{N} \left(c\boldsymbol{\alpha}_i \cdot \boldsymbol{p_i} + (\beta_i - 1)c^2 + V_{nuc}(r_i) \right) + \sum_{i>j}^{N} \frac{1}{r_{ij}}, \tag{2}$$

where $V_{nuc}(r_i)$ is the the monopole part of the electron-nucleus Coulomb interaction, r_{ij} is the distance between electrons i and j, $\boldsymbol{\alpha}$ and β are the 4-by-4 Dirac matrices, and c is the speed of light.

The approximate solutions to the wave equations are referred to as atomic state functions (ASFs). An atomic state function, $\Psi(\gamma PJ)$, is in our approach represented by a linear combination of configuration state functions(CSFs),

$$\Psi(\gamma PJ) = \sum_{j=1}^{NCSFs} c_j \Phi(\gamma_j PJ), \tag{3}$$

where P is the parity and J is the total angular momentum. γ_j represents all necessary quantum numbers and the orbital occupancy to define the CSF, while c_j are the mixing coefficients. The γ is usually selected as the γ_j corresponding to the largest weight $|c_j|^2$.

The CSFs are in turn constructed as angular-momentum-coupled, anti-symmetrized products of one-electron Dirac-orbitals of the form

$$\psi(r) = \psi_{n\kappa,m}(r) = \frac{1}{r}\begin{pmatrix} P_{n\kappa}(r)\chi_{\kappa,m}(\theta,\varphi) \\ \mathrm{i}Q_{n\kappa}(r)\chi_{-\kappa,m}(\theta,\varphi) \end{pmatrix}, \quad (4)$$

where $P_{n\kappa}(r)$ and $Q_{n\kappa}(r)$ are the large and small components of the radial wave function, and $\chi_{\pm\kappa,m}(\theta,\varphi)$ are two-component spin-orbit functions.

The extended optimal level (EOL) scheme is used to determine energies and wave functions. In the EOL scheme, the radial parts of the Dirac orbitals and the expansion coefficients of the targeted states are optimized to self-consistency by solving the MCDHF equations, which are derived using the variational approach (Dyall et al. 1989). In subsequent relativistic configuration interaction (RCI) calculations the transverse photon interaction (Breit interaction)

$$H_{Breit} = -\sum_{i<j}^{N}\left[\boldsymbol{\alpha}_i\cdot\boldsymbol{\alpha}_j\frac{\cos(w_{ij}r_{ij}/c)}{r_{ij}} + (\boldsymbol{\alpha}_i\cdot\boldsymbol{\nabla}_i)\left(\boldsymbol{\alpha}_i\cdot\boldsymbol{\nabla}_j\right)\frac{\cos(w_{ij}r_{ij}/c)-1}{w_{ij}^2 r_{ij}/c^2}\right] \quad (5)$$

may be included in the Hamiltonian (McKenzie et al. 1980). The photon frequency w_{ij}, used by the RCI program in calculating the matrix elements of the transverse photon interaction, is taken as the difference of the diagonal Lagrange multipliers associated with the orbitals. The leading quantum electrodynamic (QED) corrections effects, in the form of self-energy and vacuum polarization, are also included. The CSFs are given in the jj-coupling scheme during this procedure, but to make a comparison with experiments more feasible, we transform the resulting wave function to the LSJ-coupling scheme, using the JJ2LSJ program (Gaigalas et al. 2003, 2004, 2017) part of the GRASP2K code (Jönsson et al. 2013). All the calculations were performed with an updated parallel version of the GRASP2K code by Jönsson et al. (2013). To calculate the spin-angular part of the matrix elements, the second quantization method in coupled tensorial form and quasispin technique (Gaigalas et al. 1997, 2001) were adopted.

3.2. Computation of transition parameters

Once well-converged and effectively complete ASFs have been obtained radiative transition such as transition probabilities and weighted oscillator strengths can be determined. The transition parameters between two states γJM and $\gamma' J' M'$ are expressed in terms reduced matrix elements

$$\langle\Psi(\gamma PJ)\|\mathbf{T}\|\Psi(\gamma' P' J')\rangle = \sum_{j,k} c_j c'_k \langle\Phi(\gamma_j PJ)\|\mathbf{T}\|\Phi(\gamma'_k P' J')\rangle, \quad (6)$$

where $\mathbf{T}$ is the transition operator (Grant 1974).

For electric multipole transitions, there are two forms of the transition operator, the length (Babushkin gauge) and velocity (Coulomb gauge) forms (Grant 1974). Due to the definition of these two, the length form is more sensitive to the outer part of the wave functions, which are usually active in radiative transitions. A number of studies have shown that the length form generally gives more reliable values at a given level of valence and core–valence electron correlation although the velocity form seems to be more stable for transitions including highly excited Rydberg states (Pehlivan Rhodin et al. 2017). It is common to use the agreement between transition rates A_l and A_v computed in two forms as an indicator of accuracy of the wave functions, (see review by Froese Fischer (2009); Ekman et al. (2014)). A possible measure of this is the quantity dT, characterizing the uncertainty of the calculated transition rates and defined as

$$dT = \frac{|A_l - A_v|}{\max(A_l, A_v)}, \quad (7)$$

where A_l and A_v are the transition rates in length and velocity forms respectively. The values of dT do not represent uncertainty estimates for each individual transition but should be considered as statistical indicators of uncertainties within given sets of transitions.

4. Calculations

Our MCDHF and RCI calculations for doubly and triply ionized silicon started by defining a multireference (MR) set of configurations. From this we allow single and double substitutions to a systematically increasing active set of orbitals.

4.1. Si III

In doubly ionized silicon, calculations were performed for states belonging to the $3s^2$, the $3p^2$; the $3p4p$; the $3sns$ with $n = 4,...,9$; the $3snd$ with $n = 3,...,8$; the $3sng$ with $n = 5,...,8$ even configurations and furthermore, the $3snp$ with $n = 3,...,9$; the $3snf$ with $n = 4,...,8$; the $3pnd$ with $n = 3, 4$; and the $3p4s$ odd configurations. These configurations define the MR for the even and odd parities, respectively. Terms involving configurations with $n = 8$ and 9 do not belong to our targeted states but they are taken into account to obtain orbitals with large radii to get a reasonable agreement between length and velocity form for the transition properties, see Pehlivan Rhodin et al. (2017).

In the first step of our calculations, an initial MCDHF calculation in the EOL scheme (Dyall et al. 1989) was performed simultaneously for all even and odd multireference states. These initial calculations were followed by calculations with expansions including the configuration state functions (CSFs) obtained by single (S), double (D) substitutions of electrons from the spectroscopic reference configurations to the active set of orbitals (Olsen et al. 1988; Sturesson et al. 2007).

In an restricted active set approach (RAS) restrictions are put on the allowed substitutions from the MR, when generating the full space of CSFs. We therefore define the valence region of the atom as the two outer electrons, outside the $1s^2 2s^2 2p^6$ core subshells. We kept the $1s^2$-subshell fixed in all calculations, that is, not allowing substitutions from it. After optimizing simultaneously the even and odd states of the MR-set in the first step of calculations, our goal was to include valence-valence (VV) and core-valence (CV) interaction to convergence. We optimized four layers of correlation orbitals based on the VV correlation, only allowing SD substitutions from the valence subshells. The orbitals in the active set were systematically extended to include orbitals up to the $13s, 13p, 12d, 12f, 12g$, and $9h$ in the final correlation layer. These MCDHF calculations were followed by RCI calculations including Breit-interaction and some QED effects as described above.

As a final step of our work, an RCI calculation was performed. The expansion for that RCI calculation was obtained by augmenting the largest SD valence expansion with a CV expansion. The CV expansion was generated by SD substitutions

from the valence orbitals and the $2p^6$ core with the restriction that there should be at the most one substitution from the $2s$ or $2p$ subshells. We neglected core-core (CC) correlation, meaning more than one excitation from the core, which was comparatively unimportant for both the energy separations and the transition probabilities (Zou & Fischer 2000). The resulting expansions consisted of 1 401 150 and 1 760 209 CSFs distributed over the $J = 0, 1, ..., 6$ symmetries for even and odd parity, respectively.

4.1.1. Si IV

In triply ionized silicon, calculations were performed for states belonging to the configurations $2s^22p^6nl$ where $n \leq 9$ and $l \leq 6$, defining the MR configurations. We again added two more layers of spectroscopic orbitals, $n = 8, 9$, in comparison with the states we were targeting to get a reasonable agreement between length and velocity form for the transition properties.

As a starting point for the calculations, MCDHF calculations in the EOL scheme were performed for the even and odd parity states in the MR simultaneously. The initial calculations were followed by separate calculations in the EOL scheme for the even and odd parity states, where the CSFs were obtained by allowing SD substitutions from the configurations in the MR to active orbital sets, which were consecutively enlarged by layers of correlation orbitals. Si IV has one electron outside closed subshells, and consequently there is no VV correlation. The corrections to our results can therefore be classified as CV and CC correlations. The major effect comes from the CV correlation. The CV expansion was obtained by restricting the substitutions in such a way that only one substitution was allowed from the $2s$ or $2p$ subshells of the configurations in the MR, and no substitutions from the $1s$ shell, this means that $1s$ shell was an inactive closed core.

The active sets of orbitals for the even and odd parity states were extended by layers to include orbitals with quantum numbers $n \leq 12$ and $l \leq 6$. Each MCDHF calculation was followed by RCI calculations, including the Breit-interaction and leading QED effects. We investigated the CC correlation effects by optimizing one layer of orbitals $n = 13$ on SD from the $2s^22p^6$ core in an RCI calculation as a final step of our work. The number of CSFs in the final even and odd state expansions were approximately 995 020 and 993 501, respectively, distributed over the different J symmetries.

5. Results

5.1. Si III

We present in Table A.1 the computed excitation energies in Si III for increasing active sets of orbitals labeled with the highest principal quantum number n of the orbitals in the active set. The calculations including only VV correlation, built on three layers of correlation orbitals, is followed by finally including the CV correlation using an RCI-approach.

The computed excitation energies are in good agreement with the values from the NIST-database (Kramida et al. 2018). For the VV correlation, the mean relative difference between theory and experiment is of the order of 0.9%. The inclusion of CV correlation effects improves the energies dramatically since the values for all computed energy separations have converged.

The final excitation energies are in good agreement with the experimental ones, with a mean difference of only 0.05%. For comparison, the experimental energies from the NIST Atomic Spectra Database (Kramida et al. (2018)) and also the differences ΔE, between the observed energies and the final computed excitation energies, are given in Table A.1.

There is excellent agreement between observations and calculations for most of the levels, with a few important exceptions, due to mislabeling of levels. The NIST label classification for Si III is based on the analysis done by Toresson (1961). Since then the NIST designations for the $3p3d\ ^1P$ and the $3p4s\ ^1P$ have been interchanged as recommended by Victor et al. (1976) and Zetterberg & Magnusson (1977). The assignments for $3p3d\ ^1P$ and $3p3d\ ^1F$ levels have been questioned previously by Reistad et al. (1984) and Brage & Hibbert (1989).

If we start by investigating the $^1F^o$-levels, we note that the $3p3d\ ^1F^o$ perturbs the $3snf$ Rydberg series. This perturbation has been studied by a number of authors along the Mg-sequence (Brage & Hibbert 1989; Reistad et al. 1984; Aashamar et al. 1986). The NIST classification identifies the level at 235413 cm^{-1} as $3p3d\ ^1F$ for convenience, even though the calculated composition is 65 % $3snf$ (Fischer & Godefroid 1982). To illustrate the complexity of the situation, we show the composition of the ^1F levels in Figure 1. It is clear that the $3p3d\ ^1F$ is not the major component for any state and that the same CSF $3s5f\ ^1F^o$ is the largest component for two levels. We therefore choose to change the designation as shown in Table A.1 where these two levels are labeled as $3s5f\,^1F^o_{3\ a}$ and $3s5f\,^1F^o_{3\ b}$, respectively.

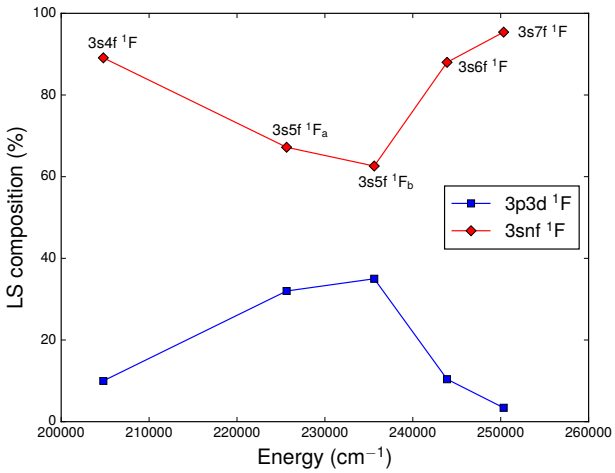

Fig. 1. $3p3d$ and $3snf$ composition of $^1F^o$ Rydberg series members.

Our second example of a strongly perturbed series investigated by Fischer & Godefroid (1982) is a short-range interaction of the plunging configuration $3p3d\ ^1P$ with the $3snp\ ^1P$ Rydberg series. In Si III the $3s6p\ ^1P_1$ and $3p3d\ ^1P_1$ are close to degenerate and the labeling of these levels is hard to reproduce. A closer look at the LS-percentage composition and excitation energies of $3snp\ ^1P$ and $3p3d\ ^1P$ are shown in Figure 2, where the level at 234923 cm^{-1} is best represented as $3p3d\ ^1P$. Also in this case we adjust the labels from NIST.

A third example of a complicated case of level-designation is the $3snd\ ^1D^e$ Rydberg series, which is perturbed by the $3p^2\ ^1D$ for low excitations and the $3p4p\ ^1D_2$ for $n = 6 - 8$. In our calculations the level energy of $3s7d\ ^1D_2$ is 247946 cm^{-1}, while the values given by NIST is 250636 cm^{-1}. However, the LS composition of the former level is 72% $3s7d\ ^1D_2$ and 18% $3p4p\ ^1D_2$. We suggest that the NIST identification of the level $^1D_2$ at 250636 cm^{-1} and at 247935 cm^{-1} should be interchanged as shown in Table A.1.

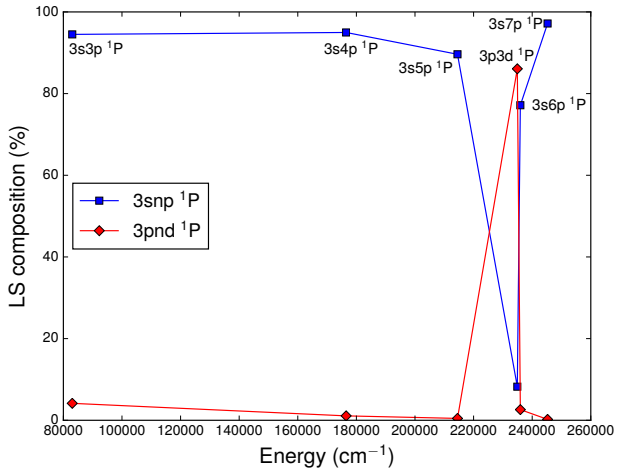

Fig. 2. $3pnd\ ^1P$ and $3snp$ composition of $^1P^o$ Rydberg series members.

A problem in spectroscopic calculations, that includes a large number of states, is to reproduce very close degeneracy between some levels. An example of this is the relative position of the singlet and triplet levels the $3snp$ Rydberg series with $n = 6-7$. It is clear that we are not able to reproduce the NIST-values for the relative position of these levels, which makes, for example, our values for intercombination lines inaccurate from the $3s6p$ and $3s7p\ ^3P$-levels.

In Table A.2, the current results for the 29 lowest excitation energies of Si III are compared with the ones from the MCHF-BP calculations by Froese Fischer et al. (2006) and *R*-matrix calculations by Del Zanna et al. (2015). To make the comparison easier the differences between observed and computed energies are also given in the last columns for the different computational approaches. From the comparison, it is clear that the agreement with the present RCI calculations and the MCHF-BP calculations is very good. Furthermore, the agreement between the current RCI results and the observed energies is improved especially above the $3p^2\ ^1S_0$ level.

The complete transition data table, using the length form of transition operator, including rates, weighted oscillator strengths, wavenumber, and the uncertainty in the computed rates, for E1 transitions in Si III for the wavelength range of 40-18239 nm is available at the CDS. The wavenumber and wavelength values are changed to match the values in the NIST database, which are the values from Reader et al. (1980). Uncertainties of the transition rates have been estimated from the expressions suggested by Ekman et al. (2014). The estimated relative uncertainties for most of the strong transitions are below 1%. For many weak transitions the uncertainties are around 10%. However, for weak intercombination transitions the uncertainties are considerably large due to difficulties in calculating the transition rates of intercombination lines. There are some weak two-electron one-photon transitions with large uncertainties. These transitions are zero in the single configuration approximation and are allowed only through correlation effects. Thus, the two-electron one-photon transitions are very difficult to compute and the uncertainties are often large.

The $3s4s\ ^1S_0 \rightarrow 3s3p\ ^1P_1$ transition is of special importance in the diagnostics of non-Maxwellian electron distributions, as discussed above. According to Dufton et al. (1983) the rate for this transition is 2.8×10^8 s^{-1}, while Nussbaumer (1986) predicted 4.0×10^8 s^{-1} and Del Zanna et al. (2015) 2.96×10^8 s^{-1}. Our result for this rate is 8.53×10^8 s^{-1} close to Froese Fischer et al. (2006) calculation of 8.99×10^8 s^{-1}.

Our estimated lifetimes (including only E1-transitions) for excited states of Si III are given in Table A.3. We also compare our results to available measurements in this table. Berry et al. (1971), Livingston et al. (1976b) and Bashkin et al. (1980) measured the lifetimes for a few levels in Si III with the beam foil method. The agreement between the current RCI results and measurements is quite satisfactory, though the results from the measurements of Berry et al. (1971) slightly differ from the RCI values. This may be explained by the uncertainties in the beam-foil method discussed by Zou et al. (1999). The lifetimes from the current RCI calculations are also compared to results from the MCHF-BP calculations by Froese Fischer et al. (2006) and MBPT calculations by Safronova et al. (2000), when these include all important transitions from a given state. The overall agreement is good, giving us confidence in the present results. For most states there is no major discrepancy between the current results and MBPT results except for the $3p3d\ ^3F^0_{2,3,4}$ states. The reason for that is unclear, but for the rest of the states the discrepancies are quite small.

5.2. Si IV

In Table A.4, we present the level energies of the lowest 45 levels in Si IV as functions of increasing active sets of orbitals (labeled by the highest principal quantum number n). The calculations are based on CV correlation, including three layers of correlation orbitals. From the inspection of Table A.4, it is clear that the present calculations are well converged with respect to the increasing orbital set. The inclusion of CC correlation effects, adding one more layer of correlation orbitals with $n = 13$, improves the energies and the final energies are in good agreement with experiment displaying a mean difference of 0.09%. We present the experimental level energies from the NIST-database for Si IV in Table A.4, including the differences between the observed and the computed energies. In Table A.4, we also compare the present computed excitation energies with those from the non-orthogonal B-spline CI method (Zatsarinny & Fischer 2002) by Froese Fischer et al. (2006) for Si IV, showing excellent agreement.

The complete transition data table, using the length form of transition operator, including rates, weighted oscillator strengths, wavenumber, and the uncertainty in the computed rates, for E1 transitions in Si IV for the wavelength range of 31-11933 nm can be found at the CDS. Uncertainties of the transition rates have been estimated from the expressions suggested by Ekman et al. (2014). The wavelength and wavenumber values are changed to match the values in the NIST database, which are the values from Reader et al. (1980). In general, the estimated relative uncertainties for most of the transitions are less than 10%. However, for some transitions the uncertainties are very large mostly due to difficulties in calculating the transition rates of intercombination lines and two-electron transitions.

Table A.5 presents our estimated lifetimes of the excited states (including only E1-transitions) in both length and velocity forms. The average relative difference between lifetimes in two forms is $\sim 0.8\%$, which is highly satisfactory. This difference might be considered to be an internal validation of the accuracy of the calculations. The comparison of our results with previously reported theoretical and experimental values are also given in Table A.5. Siems et al. (2001) performed a HFR approach to estimate the lifetimes for Si IV. In that approach, the elec-

trostatic parameters were optimized using a least-squares procedure. Berry et al. (1971) and later Bashkin et al. (1980) measured lifetimes using the beam-foil method. The overall agreement between these measured lifetimes and the current lifetimes is rather good. From the table, one can see that our results are in excellent agreement with the results of Froese Fischer et al. (2006) and Siems et al. (2001).

6. Conclusions

In this work, we performed self-consistent MCDHF and subsequent RCI calculations for Si III and Si IV, as an extension and update to earlier calculations. Previous theoretical and experimental data were used to validate our results. Excitation energies from the RCI calculations are in a very good agreement with available observations. Our present study is an extension to the most accurate MCHF-BP and the BSR_CI calculations, and in general in excellent agreements with them. The presented results significantly increase the amount of accurate energy data of astrophysical interest for the two Si-ions. The highly accurate atomic data helps to correct interpretation of the lines. Therefore, we recommend our present results based on a fully relativistic method for abundance analysis and plasma diagnostics.

Acknowledgements. Betül Atalay acknowledges financial support from the Scientific and Technological Research Council of Turkey (TUBITAK) - BIDEB 2219 International Post-Doctoral Research Fellowship Program. Tomas Brage, Per Jönsson, and Henrik Hartman acknowledge support from the Swedish Research Council (VR) under contract No.2015-04842. Dr Atalay also would like to express her appreciation of the hospitality shown by the Division of Mathematical Physics at Lund University and by the Department of Materials Science and Applied Mathematics at Malmö University.

References

Aashamar, K., Luke, T. M., & Talman, J. D. 1986, Physica Scripta, 34, 386
Aggarwal, K. M. 2017, Atomic Data and Nuclear Data Tables, 117-118, 320
Almaraz, M. A., Hibbert, A., Lavín, C., Martín, I., & Bell, K. L. 2000, Journal of Physics B: Atomic, Molecular and Optical Physics, 33, 3277
Bailey, J. D. & Landstreet, J. D. 2013, A&A, 551, A30
Bashkin, S., Astner, G., Mannervik, S., et al. 1980, Phys. Scr, 21, 820
Becker, S. R. & Butler, K. 1990, A&A, 235, 326
Berry, H. G., Bromander, J., Curtis, L. J., & Buchta, R. 1971, Physica Scripta, 3, 125
Brage, T. & Hibbert, A. 1989, Journal of Physics B: Atomic, Molecular and Optical Physics, 22, 713
Butler, K., Mendoza, C., & Zeippen, C. J. 1993, Journal of Physics B: Atomic, Molecular and Optical Physics, 26, 4409
Catanzaro, G., Leone, F., Busá, I., & Romano, P. 2008, New Astronomy, 13, 113
Cowpe, J., Astin, J., Pilkington, R., & Hill, A. 2008, Spectrochimica Acta Part B: Atomic Spectroscopy, 63, 1066 , a collection of papers presented at the Euro Mediterranean Symposium on Laser Induced Breakdown Spectroscopy (EMSLIBS 2007)
Del Zanna, G., Fernández-Menchero, L., & Badnell, N. R. 2015, A&A, 574, A99
Dufton, P. L., Hibbert, A., Kingston, A. E., & Doschek, G. A. 1983, ApJ, 274, 420
Dyall, K. G., Grant, I. P., Johnson, C. T., Parpia, F. A., & Plummer, E. P. 1989, Computer Physics Communications, 55, 425
Dzifčáková, E. & Kulinová, A. 2011, A&A, 531, A122
Ekman, J., Godefroid, M., & Hartman, H. 2014, Atoms, 2, 215
Fischer, C. F. & Godefroid, M. 1982, Physica Scripta, 25, 394
Froese Fischer, C. 2009, Physica Scripta Volume T, 134, 014019
Froese Fischer, C., Godefroid, M., Brage, T., Jönsson, P., & Gaigalas, G. 2016, Journal of Physics B Atomic Molecular Physics, 49, 182004
Froese Fischer, C., Tachiev, G., & Irimia, A. 2006, Atomic Data and Nuclear Data Tables, 92, 607
Gaigalas, G., Fischer, C., Rynkun, P., & Jönsson, P. 2017, Atoms, 5, 6
Gaigalas, G., Fritzsche, S., & Grant, I. P. 2001, Computer Physics Communications, 139, 263
Gaigalas, G., Rudzikas, Z., & Froese Fischer, C. 1997, Journal of Physics B Atomic Molecular Physics, 30, 3747
Gaigalas, G., Žalandauskas, T., & Rudzikas, Z. 2003, Atomic Data and Nuclear Data Tables, 84, 99
Gaigalas, G., Zalandauskas, T., & Fritzsche, S. 2004, Computer Physics Communications, 157, 239
Grant, I. 2007, Relativistic Quantum Theory of Atoms and Molecules: Theory and Computation, Springer Series on Atomic, Optical, and Plasma Physics (Springer)
Grant, I. P. 1974, Journal of Physics B Atomic Molecular Physics, 7, 1458
Gu, M. F. 2008, Canadian Journal of Physics, 86, 675
Hibbert, A. 1975, Computer Physics Communications, 9, 141
Iijima, T. & Nakanishi, H. 2008, A&A, 482, 865
Iorga, C. & Stancalie, V. 2018, Atomic Data and Nuclear Data Tables, 123-124, 313
Jönsson, P., Gaigalas, G., Bieroń, J., Fischer, C. F., & Grant, I. P. 2013, Computer Physics Communications, 184, 2197
Keenan, F. P., Cook, J. W., Dufton, P. L., & Kingston, A. E. 1989, ApJ, 340, 1135
Kelleher, D. E. & Podobedova, L. I. 2008, Journal of Physical and Chemical Reference Data, 37, 1285
Kramida, A., Yu. Ralchenko, Reader, J., & and NIST ASD Team. 2018, NIST Atomic Spectra Database (ver. 5.5.6), [Online]. Available: https://physics.nist.gov/asd [2015, April 16]. National Institute of Standards and Technology, Gaithersburg, MD.
Kwong, H. S., Johnson, B. C., Smith, P. L., & Parkinson, W. H. 1983, Physical Review A, 27, 3040
Livingston, A. E., Baudinet-Robinet, Y., Garnir, H. P., & Dumont, P. D. 1976a, J. Opt. Soc. Am., 66, 1393
Livingston, A. E., Kernahan, J. A., Irwin, D. J. G., & Pinnington, E. H. 1976b, Journal of Physics B: Atomic and Molecular Physics, 9, 389
Maniak, S., Träbert, E., & Curtis, L. 1993, Physics Letters A, 173, 407
McKenzie, B. J., Grant, I. P., & Norrington, P. H. 1980, Computer Physics Communications, 21, 233
Monteverde, M. I., Herrero, A., & Lennon, D. J. 2000, ApJ, 545, 813
Nandy, D. K. & Sahoo, B. K. 2015, MNRAS, 447, 3812
Nieva, M. F. & Przybilla, N. 2012, A&A, 539, A143
Nussbaumer, H. 1986, A&A, 155, 205
Ogilvie, R. E. & Nicolich, J. 2009, Spectrochimica Acta Part B: Atomic Spectroscopy, 64, 788 , a Collection of Papers Presented at the 19th International Congress on X-Ray Optics and Microanalysis (ICXOM-19)
Ojha, P. C., Keenan, F. P., & Hibbert, A. 1988, Journal of Physics B Atomic Molecular Physics, 21, L395
Olsen, J., Roos, B. O., Jørgensen, P., & Jensen, H. J. A. 1988, J. Chem. Phys., 89, 2185
Pehlivan Rhodin, A. 2018, PhD thesis, Lund University
Pehlivan Rhodin, A., Hartman, H., Nilsson, H., & Jönsson, P. 2017, A&A, 598, A102
Pinfield, D. J., Keenan, F. P., Mathioudakis, M., et al. 1999, The Astrophysical Journal, 527, 1000
Przybilla, N., Nieva, M.-F., & Butler, K. 2008, The Astrophysical Journal Letters, 688, L103
Reader, J., Corliss, C. H., Wiese, W. L., & Martin, G. A. 1980, Wavelengths and transition probabilities for atoms and atomic ions: Part 1. Wavelengths, part 2. Transition probabilities (U.S. Government Printing Office)
Reistad, N., Brage, T., Ekberg, J. O., & Engström, L. 1984, Physica Scripta, 30, 249
Rubin, R. H., Dufour, R. J., & Walter, D. K. 1993, ApJ, 413, 242
Safronova, M. S., Derevianko, A., & Johnson, W. R. 1998, Phys. Rev. A, 58, 1016
Safronova, U. I., Johnson, W. R., & Berry, H. G. 2000, Phys. Rev. A, 61, 052503
Seaton, M. J. 1987, Journal of Physics B: Atomic and Molecular Physics, 20, 6363
Siegel, W., Migdalek, J., & Kim, Y.-K. 1998, Atomic Data and Nuclear Data Tables, 68, 303
Siems, A., Luna, F., & Trigueiros, A. 2001, Journal of Quantitative Spectroscopy and Radiative Transfer, 68, 635
Simón-Díaz, S. 2010, A&A, 510, A22
Sturesson, L., Jönsson, P., & Froese Fischer, C. 2007, Computer Physics Communications, 177, 539
Theodosiou, C. E. & Curtis, L. J. 1988, Phys. Rev. A, 38, 4435
Toresson, Y. G. 1961, Ark. Fys. (Stockholm), 18, 389
Victor, G. A., Stewart, R. F., & Laughlin, C. 1976, ApJS, 31, 237
Yamazaki, H., Yoshiki, M., Takemura, M., Tomita, M., & Takeno, S. 2009, Spectrochimica Acta Part B: Atomic Spectroscopy, 64, 808 , a Collection of Papers Presented at the 19th International Congress on X-Ray Optics and Microanalysis (ICXOM-19)
Zatsarinny, O. & Fischer, C. F. 2002, Journal of Physics B: Atomic, Molecular and Optical Physics, 35, 4669
Zetterberg, P. O. & Magnusson, C. E. 1977, Physica Scripta, 15, 189
Zou, Y. & Fischer, C. F. 2000, Phys. Rev. A, 62, 062505
Zou, Y., Hutton, R., Huldt, S., et al. 1999, Physica Scripta Volume T, 80, 460

Appendix A: Additional Tables

Table A.1. Computed excitation energies in cm $^{-1}$ for Si III from different computational models. The differences ΔE between the final computations and the observed values are shown in the last column.

	VV						
Level	$n = 10$	$n = 11$	$n = 12$	$n = 13$	CV	$E_{\rm obs}$ [a]	ΔE
$3s^2\ ^1S_0$	0	0	0	0	0	0	0
$3s3p\ ^3P^o_0$	51539	51541	51561	51604	52790	52725	-65
$3s3p\ ^3P^o_1$	51656	51671	51686	51728	52913	52853	-60
$3s3p\ ^3P^o_2$	51893	51938	51941	51981	53164	53115	-49
$3s3p\ ^1P^o_1$	83380	83186	83145	83094	83031	82884	-147
$3p^2\ ^1D_2$	120291	120305	120314	120361	122447	122215	-232
$3p^2\ ^3P_0$	128668	128658	128667	128703	129832	129708	-124
$3p^2\ ^3P_1$	128808	128794	128796	128832	129953	129842	-111
$3p^2\ ^3P_2$	129043	129052	129046	129080	130193	130101	-92
$3s3d\ ^3D_3$	141773	141743	141761	141794	143106	142944	-162
$3s3d\ ^3D_2$	142183	141743	141762	141805	143162	142946	-216
$3s3d\ ^3D_1$	142470	141743	141762	141812	143208	142948	-260
$3s4s\ ^3S_1$	151757	151808	151821	151875	153332	153377	45
$3p^2\ ^1S_0$	153325	152950	152897	152824	153953	153444	-509
$3s4s\ ^1S_0$	157694	157704	157698	157701	159065	159070	5
$3s3d\ ^1D_2$	166150	165215	165198	165172	166013	165765	-248
$3s4p\ ^3P^o_0$	173433	173475	173497	173551	175219	175230	11
$3s4p\ ^3P^o_1$	173464	173511	173530	173582	175247	175263	16
$3s4p\ ^3P^o_2$	173533	173589	173601	173648	175312	175336	24
$3s4p\ ^1P^o_1$	174860	174906	174918	174952	176503	176487	-16
$3p3d\ ^3F^o_2$	196943	196419	196441	196496	199259	198923	-336
$3p3d\ ^3F^o_3$	196787	196519	196539	196589	199318	199026	-292
$3p3d\ ^3F^o_4$	196622	196651	196670	196713	199402	199164	-238
$3s4d\ ^3D_1$	199846	199861	199884	199920	201691	201598	-93
$3s4d\ ^3D_2$	200003	199857	199881	199928	201666	201598	-68
$3s4d\ ^3D_3$	200134	199855	199879	199934	201634	201599	-35
$3s4d\ ^1D_2$	202714	202640	202662	202713	204464	204331	-133
$3s4f\ ^1F^o_3$	203063	202705	202716	202733	204795	204828	33
$3p3d\ ^1D^o_2$	203175	202977	202996	203047	205357	205029	-328
$3s5s\ ^3S_1$	204234	204288	204303	204359	206118	206176	58
$3s5s\ ^1S_0$	205920	205971	205988	206039	207828	207874	46
$3s4f\ ^3F^o_2$	207666	207551	207571	207627	209597	209531	-66
$3s4f\ ^3F^o_3$	207622	207578	207597	207652	209612	209559	-53
$3s4f\ ^3F^o_4$	207574	207616	207635	207687	209637	209600	-37
$3s5p\ ^1P^o_1$	212511	212566	212587	212639	214504	214532	28
$3s5p\ ^3P^o_2$	213130	213157	213173	213213	214998	214989	-9
$3s5p\ ^3P^o_1$	213159	213142	213163	213212	215002	214995	-7
$3s5p\ ^3P^o_0$	213160	213133	213157	213210	215005	214995	-10
$3p3d\ ^3P^o_2$	214375	214269	214285	214319	216450	216190	-260
$3p3d\ ^3P^o_1$	214967	214376	214391	214431	216613	216289	-324
$3p3d\ ^3P^o_0$	215325	214440	214453	214496	216717	216350	-367
$3p3d\ ^3D^o_1$	216019	215773	215793	215839	217724	217386	-338
$3p3d\ ^3D^o_2$	216518	215881	215898	215925	217743	217440	-303
$3p3d\ ^3D^o_3$	216356	215827	215845	215884	217736	217489	-247
$3s5f\ ^1F^o_3$ [a]	224092	223605	223620	223633	225644	225526	-118
$3p4s\ ^3P^o_0$	224260	224260	224273	224322	226479	226400	-79
$3p4s\ ^3P^o_1$	224376	224389	224397	224445	226597	226527	-70
$3p4s\ ^3P^o_2$	224636	224676	224677	224724	226884	226820	-64
$3s5d\ ^3D_1$	225236	225165	225187	225232	227105	227081	-24
$3s5d\ ^3D_2$	225179	225159	225181	225230	227092	227084	-8
$3s5d\ ^3D_3$	225124	225154	225177	225226	227076	227089	13
$3s5d\ ^1D_2$	225833	225714	225733	225773	227695	227665	-30
$3p4s\ ^1P^o_1$	226814	226801	226778	226775	228788	228700	-88

Table A.1. continued.

	VV						
Level	$n = 10$	$n = 11$	$n = 12$	$n = 13$	CV	$E_{\rm obs}{}^a$	ΔE
$3s6s\ ^3S_1$	227576	227630	227648	227703	229556	229623	67
$3s5f\ ^3F^o_2$	228134	228194	228207	228265	230201	230268	67
$3s5f\ ^3F^o_3$	228133	228194	228206	228264	230201	230269	68
$3s5f\ ^3F^o_4$	228134	228195	228217	228265	230201	230271	70
$3s5g\ ^3G_3$	228135	228196	228219	228266	230230	230301	71
$3s5g\ ^3G_4$	228159	228208	228231	228288	230232	230302	70
$3s5g\ ^1G_4$	228176	228211	228233	228289	230233	230302	69
$3s5g\ ^3G_5$	228169	228209	228232	228288	230232	230302	70
$3s6s\ ^1S_0$	228303	228359	228378	228433	230301	230364	63
$3s6p\ ^3P^o_0$	232356	232413	232437	232493	234359	234415	56
$3s6p\ ^3P^o_1$	232364	232423	232446	232501	234365	234428	63
$3s6p\ ^3P^o_2$	232382	232443	232464	232518	234381	234442	61
$3p3d\ ^1P^{o*}_1$	233982	233003	232982	232927	234923	234388	-535
$3s5f\ ^1F^o_{3\,b}$	234526	233780	233783	233763	235612	235414	-198
$3s6p\ ^1P^{o*}_1$	234522	234025	234033	234066	235957	235951	-6
$3s6d\ ^3D_1$	238206	238220	238231	238287	240267	240262	-5
$3s6d\ ^3D_2$	238211	238245	238256	238308	240278	240284	6
$3s6d\ ^3D_3$	238224	238280	238291	238338	240297	240315	18
$3s6d\ ^1D_2$	238470	238484	238498	238548	240537	240550	13
$3s7s\ ^3S_1$	240049	240105	240124	240179	242075	242145	70
$3s6f\ ^3F^o_2$	240282	240327	240352	240410	242336	242411	75
$3s6f\ ^3F^o_3$	240277	240328	240352	240409	242335	242411	76
$3s6f\ ^3F^o_4$	240271	240328	240352	240408	242335	242412	77
$3s6g\ ^3G_3$	240301	240363	240387	240440	242400	242474	74
$3s6g\ ^3G_4$	240300	240364	240385	240441	242403	242474	71
$3s6g\ ^1G_4$	240302	240365	240388	240443	242405	242474	69
$3s6g\ ^3G_5$	240301	240365	240386	240443	242405	242475	70
$3s7s\ ^1S_0$	240428	240487	240508	240564	242466	242538	72
$3p4p\ ^1P_1$	240550	240603	240625	240679	242992	242885	-107
$3s6f\ ^1F^o_3$	242239	241980	241993	242017	243896	243869	-28
$3p4p\ ^3D_1$	242550	242573	242548	242602	244839	244737	-102
$3s7p\ ^3P^o_0$	242822	242881	242906	242962	244862	244929	67
$3s7p\ ^3P^o_1$	242827	242887	242910	242966	244866	244933	67
$3s7p\ ^3P^o_2$	242836	242898	242920	242975	244874	244943	69
$3p4p\ ^3D_2$	242665	242699	242671	242723	244966	244866	-100
$3p4p\ ^3D_3$	242864	242913	242881	242930	245194	245087	-107
$3s7p\ ^1P^o_1$	243236	243291	243313	243364	245250	244871	-379
$3s7d\ ^1D_2$	245752	245805	245777	245829	247946	247935	-11
$3p4p\ ^3P_0$	245541	245588	245603	245649	247965	247872	-93
$3p4p\ ^3P_1$	245626	245675	245685	245729	248040	247954	-86
$3p4p\ ^3P_2$	245863	245922	245910	245956	248239	248168	-71
$3p4p\ ^3S_1$	246598	246609	246619	246665	248952	248773	-179
$3s7d\ ^3D_1$	247056	247068	247092	247148	249067	249094	27
$3s7d\ ^3D_2$	247050	247079	247102	247152	249068	249104	36
$3s7d\ ^3D_3$	247045	247096	247118	247160	249074	249121	47
$3s7f\ ^3F^o_2$	247629	247682	247707	247765	249698	249774	76
$3s7f\ ^3F^o_3$	247626	247683	247707	247764	249697	249775	78
$3s7f\ ^3F^o_4$	247622	247683	247707	247763	249696	249775	79
$3s7g\ ^3G_3$	247648	247711	247730	247786	249743	249817	74
$3s7g\ ^3G_4$	247647	247711	247729	247787	249746	249818	72
$3s7g\ ^1G_4$	247649	247712	247732	247787	249747	249818	71
$3s7g\ ^3G_5$	247648	247712	247730	247788	249747	249819	72
$3s7f\ ^1F^o_3$	248401	248352	248371	248415	250333	250366	33

Notes. * Labeling is changed from NIST-standard to better represent the composition of different levels in a Rydberg series, according to our calculations. As an example are two levels labeled with the same $3s5f\ ^1F$ term but different indices are used to distinguish them. Details are given in the text.

References. [(a)]Kramida et al. (2018).

Table A.2. Observed and computed excitation energies for the 29 lowest states in Si III, from present calculations ($E_{\rm RCI}$) and other theoretical results ($E^{c,d}_{\rm theor}$). These are compared to values from the NIST-database ($E^{b}_{\rm obs}$). ΔE represents the difference between observed and computed energies. All energies are given in $\rm cm^{-1}$.

Level	$E^{a}_{\rm RCI}$	$E^{b}_{\rm obs}$	$E^{c}_{\rm theor}$	$E^{d}_{\rm theor}$	$\Delta E^{a}_{\rm RCI}$	$\Delta E^{c}_{\rm theor}$	$\Delta E^{d}_{\rm theor}$
$3s^2\ ^1S_0$	0	0	0	0	0	0	0
$3s3p\ ^3P^o_0$	52790	52725	52704	51156	-65	20	1568
$3s3p\ ^3P^o_1$	52913	52853	52835	51267	-60	18	1586
$3s3p\ ^3P^o_2$	53164	53115	53099	51491	-49	16	1624
$3s3p\ ^1P^o_1$	83031	82884	83069	84060	-147	-185	-1176
$3p^2\ ^1D_2$	122447	122215	122487	120194	-232	-273	2020
$3p^2\ ^3P_0$	129832	129708	129751	128551	-124	-43	1157
$3p^2\ ^3P_1$	129953	129842	129891	128664	-111	-50	1177
$3p^2\ ^3P_2$	130193	130101	130153	128886	-92	-53	1214
$3s3d\ ^3D_3$	143106	142944	143640	142257	-162	-697	686
$3s3d\ ^3D_2$	143162	142946	143638	142252	-216	-693	693
$3s3d\ ^3D_1$	143208	142948	143644	142249	-260	-696	699
$3s4s\ ^3S_1$	153332	153377	153881	151563	45	-504	1814
$3p^2\ ^1S_0$	153953	153444	153855	155103	-509	-411	-1659
$3s4s\ ^1S_0$	159065	159070	159604	159383	5	-535	-314
$3s3d\ ^1D_2$	166013	165765	166490	168327	-248	-725	-2562
$3s4p\ ^3P^o_0$	175219	175230	175704	174006	11	-474	1224
$3s4p\ ^3P^o_1$	175247	175263	175743	174036	16	-480	1227
$3s4p\ ^3P^o_2$	175312	175336	175821	174102	24	-485	1234
$3s4p\ ^1P^o_1$	176503	176487	176963	175288	-16	-476	1199
$3p3d\ ^3F^o_2$	199259	198923	199701		-336	-778	
$3p3d\ ^3F^o_3$	199318	199026	199811		-292	-785	
$3p3d\ ^3F^o_4$	199402	199164	199955		-238	-791	
$3s4d\ ^3D_1$	201691	201598	202258		-93	-661	
$3s4d\ ^3D_2$	201666	201598	202263		-68	-665	
$3s4d\ ^3D_3$	201634	201599	202265		-35	-666	
$3s4d\ ^1D_2$	204464	204331	205114		-133	-784	
$3s4f\ ^1F^o_3$	204795	204829	205537		33	-709	
$3p3d\ ^1D^o_2$	205357	205029	205765		-328	-736	

References. [(a)]Present calculations;[(b)]Kramida et al. (2018); [(c)]Froese Fischer et al. (2006); [(d)]Del Zanna et al. (2015).

Table A.3. Results for Si III: Comparison between computed lifetimes, in length (τ_l) and velocity (τ_v) gauge, from our calculations. These are compared to the predicted lifetimes from MCHF-BP[b] ($\tau_{\text{MCHF-BP}}$) and MBPT[c] (τ_{MBPT}) models, as well as experimental results $\tau^{d,e}_{\text{obs}}$, with stated uncertainties. All values are given in seconds.

	RCI[a]					
Level	τ_l	τ_v	$\tau_{\text{MCHF-BP}}$[b]	τ_{MBPT}[c]	τ_{obs}[d]	τ_{obs}[e]
$3s3p\ ^3P^o_1$	7.679E-05	7.822E-05	5.809E-05	1.010E-04		
$3s3p\ ^1P^o_1$	4.024E-10	4.010E-10	4.050E-10	4.290E-10		(4 ± 1)E-10
$3p^2\ ^1D_2$	3.438E-08	3.331E-08	3.273E-08	4.570E-08	(2.60 ± 0.15)E-08	(2.6 ± 0.3)E-08
$3p^2\ ^3P_0$	4.747E-10	4.726E-10	4.779E-10	4.650E-10	(5.0 ± 0.3)E-10[f]	(3.4 ± 1.0)E-10
$3p^2\ ^3P_1$	4.735E-10	4.714E-10	4.764E-10	4.740E-10	(5.0 ± 0.3)E-10[f]	(3.4 ± 1.0)E-10
$3p^2\ ^3P_2$	4.715E-10	4.693E-10	4.741E-10	4.210E-10	(5.0 ± 0.3)E-10[f]	(3.4 ± 1.0)E-10
$3s3d\ ^3D_3$	3.564E-10	3.564E-10	3.524E-10	3.770E-10		
$3s3d\ ^3D_2$	3.540E-10	3.545E-10	3.506E-10	3.740E-10		
$3s3d\ ^3D_1$	3.523E-10	3.531E-10	3.494E-10	3.740E-10		
$3s4s\ ^3S_1$	4.069E-10	4.078E-10	4.068E-10			
$3p^2\ ^1S_0$	4.328E-10	4.306E-10	4.440E-10	4.760E-10	(5.8 ± 0.4)E-10[f]	
$3s4s\ ^1S_0$	1.172E-09	1.178E-09	1.112E-09			
$3s3d\ ^1D_2$	2.185E-10	2.186E-10	2.170E-10	2.320E-10		
$3s4p\ ^3P^o_0$	3.400E-09	3.422E-09	3.409E-09		(3.3 ± 0.3)E-09	(4.1 ± 0.5)E-09
$3s4p\ ^3P^o_1$	3.385E-09	3.403E-09	3.390E-09		(3.6 ± 0.3)E-09	(4.5 ± 0.5)E-09
$3s4p\ ^3P^o_2$	3.367E-09	3.375E-09	3.373E-09			
$3s4p\ ^1P^o_1$	1.972E-09	1.992E-09	1.926E-09			
$3p3d\ ^3F^o_2$	9.971E-07	1.160E-06	1.124E-06	0.023E-06		
$3p3d\ ^3F^o_3$	8.869E-07	1.004E-06	2.210E-06	0.025E-06		
$3p3d\ ^3F^o_4$	9.678E-07	1.272E-06	2.378E-06	0.026E-06		
$3s4d\ ^3D_3$	2.871E-09	2.872E-09	2.818E-09		(3.3 ± 0.3)E-09	(4.0 ± 0.4)E-09
$3s4d\ ^3D_2$	2.837E-09	2.846E-09	2.797E-09		(3.3 ± 0.3)E-09	(4.0 ± 0.4)E-09
$3s4d\ ^3D_1$	2.814E-09	2.829E-09	2.783E-09		(3.3 ± 0.3)E-09	(4.0 ± 0.4)E-09
$3s4d\ ^1D_2$	1.263E-09	1.270E-09	1.294E-09		(1.25 ± 0.15)E-09	(1.9 ± 0.3)E-09
$3s4f\ ^1F^o_3$	6.169E-10	6.185E-10	5.979E-10			
$3p3d\ ^1D^o_2$	4.277E-10	4.273E-10	4.263E-10	3.800E-10		
$3s5s\ ^3S_1$	7.438E-10	7.467E-10				
$3s5s\ ^1S_0$	1.111E-09	1.114E-09				
$3s4f\ ^3F^o_2$	4.795E-10	4.788E-10			(5.1 ± 0.3)E-10[f]	(12 ± 1)E-10
$3s4f\ ^3F^o_3$	4.793E-10	4.786E-10			(5.1 ± 0.3)E-10[f]	(12 ± 1)E-10
$3s4f\ ^3F^o_4$	4.790E-10	4.780E-10			(5.1 ± 0.3)E-10[f]	(12 ± 1)E-10
$3s5p\ ^1P^o_1$	1.279E-09	1.288E-09				
$3s5p\ ^3P^o_2$	2.270E-09	2.276E-09				
$3s5p\ ^3P^o_1$	2.875E-09	2.889E-09				
$3s5p\ ^3P^o_0$	3.253E-09	3.273E-09				
$3p3d\ ^3P^o_2$	3.216E-10	3.225E-10				
$3p3d\ ^3P^o_1$	3.096E-10	3.110E-10				
$3p3d\ ^3P^o_0$	3.056E-10	3.076E-10				
$3p3d\ ^3D^o_1$	2.016E-10	2.025E-10				(3.6 ± 0.4)E-10
$3p3d\ ^3D^o_3$	2.020E-10	2.023E-10				(3.6 ± 0.4)E-10
$3p3d\ ^3D^o_2$	2.023E-10	2.028E-10				(3.6 ± 0.4)E-10
$3s5f\ ^1F^o_3$ [a]	4.807E-10	4.824E-10				(10 ± 5)E-10
$3p4s\ ^3P^o_0$	4.548E-10	4.538E-10				
$3p4s\ ^3P^o_1$	4.520E-10	4.511E-10				
$3p4s\ ^3P^o_2$	4.474E-10	4.468E-10				
$3s5d\ ^3D_3$	8.682E-09	8.748E-09				
$3s5d\ ^3D_2$	8.646E-09	8.735E-09				
$3s5d\ ^3D_1$	8.617E-09	8.734E-09				
$3s5d\ ^1D_2$	5.794E-09	5.833E-09				
$3p4s\ ^1P^o_1$	4.245E-10	4.246E-10				
$3s6s\ ^3S_1$	1.285E-09	1.291E-09				
$3s5f\ ^3F^o_3$	9.537E-10	9.544E-10				(14 ± 2)E-10
$3s5f\ ^3F^o_2$	9.555E-10	9.566E-10				(14 ± 2)E-10

Table A.3. continued.

Level	RCI[a]		$\tau_{\text{MCHF-BP}}$[b]	τ_{MBPT}[c]	τ_{obs}[d]	τ_{obs}[e]
	τ_l	τ_v				
$3s5f\ ^3F^o_4$	9.511E-10	9.517E-10				(14 ± 2)E-10
$3s5g\ ^3G_3$	2.775E-09	2.772E-09				(4.3 ± 0.5)E-09
$3s5g\ ^3G_4$	2.776E-09	2.773E-09				(4.3 ± 0.5)E-09
$3s5g\ ^3G_5$	2.775E-09	2.773E-09				(4.3 ± 0.5)E-09
$3s5g\ ^1G_4$	2.779E-09	2.774E-09				
$3s6s\ ^1S_0$	1.810E-09	1.815E-09				
$3s6p\ ^3P^o_0$	9.157E-09	9.335E-09				
$3s6p\ ^3P^o_1$	8.981E-09	9.117E-09				
$3s6p\ ^3P^o_2$	9.032E-09	9.105E-09				
$3p3d\ ^1P^o_1$	2.809E-10	2.843E-10				
$3s5f\ ^1F^o_3$ [b]	3.995E-10	4.003E-10				
$3s6p\ ^1P^o_1$	1.129E-09	1.136E-09				
$3s6d\ ^3D_1$	5.243E-09	5.354E-09				
$3s6d\ ^3D_2$	5.548E-09	5.645E-09				
$3s6d\ ^3D_3$	5.953E-09	6.035E-09				
$3s6d\ ^1D_2$	1.081E-08	1.095E-08				
$3s7s\ ^3S_1$	2.009E-09	2.021E-09				
$3s6f\ ^3F^o_4$	1.676E-09	1.679E-09				
$3s6f\ ^3F^o_3$	1.684E-09	1.687E-09				
$3s6f\ ^3F^o_2$	1.690E-09	1.695E-09				
$3s6g\ ^3G_3$	4.764E-09	4.748E-09				
$3s6g\ ^3G_4$	4.782E-09	4.763E-09				
$3s6g\ ^1G_4$	4.802E-09	4.793E-09				
$3s6g\ ^3G_5$	4.759E-09	4.754E-09				
$3s7s\ ^1S_0$	2.849E-09	2.859E-09				
$3p4p\ ^1P_1$	6.436E-10	6.446E-10				
$3s6f\ ^1F^o_3$	8.651E-10	8.659E-10				
$3p4p\ ^3D_1$	7.732E-10	7.724E-10				
$3s7p\ ^3P^o_0$	1.524E-08	1.561E-08				
$3s7p\ ^3P^o_1$	1.521E-08	1.551E-08				
$3s7p\ ^3P^o_2$	1.518E-08	1.535E-08				
$3p4p\ ^3D_2$	7.715E-10	7.714E-10				
$3p4p\ ^3D_3$	7.665E-10	7.664E-10				
$3s7p\ ^1P^o_1$	7.755E-09	7.978E-09				
$3s7d\ ^1D_2$	3.670E-09	3.710E-09				
$3p4p\ ^3P_0$	7.308E-10	7.301E-10				
$3p4p\ ^3P_1$	7.334E-10	7.326E-10				
$3p4p\ ^3P_2$	7.504E-10	7.493E-10				
$3p4p\ ^3S_1$	9.027E-10	9.046E-10				
$3s7d\ ^3D_1$	6.279E-09	6.118E-09				
$3s7d\ ^3D_2$	5.964E-09	5.850E-09				
$3s7d\ ^3D_3$	5.550E-09	5.492E-09				
$3s7f\ ^3F^o_4$	2.689E-09	2.697E-09				
$3s7f\ ^3F^o_3$	2.708E-09	2.718E-09				
$3s7f\ ^3F^o_2$	2.722E-09	2.736E-09				
$3s7g\ ^3G_3$	7.614E-09	7.543E-09				
$3s7g\ ^3G_4$	7.632E-09	7.616E-09				
$3s7g\ ^1G_4$	7.804E-09	7.727E-09				
$3s7g\ ^3G_5$	7.610E-09	7.609E-09				
$3s7f\ ^1F^o_3$	1.713E-09	1.723E-09				

References. [(a)]Present calculations; [(b)]Froese Fischer et al. (2006); [(c)]Safronova et al. (2000); [(d)]Bashkin et al. (1980); [(e)]Berry et al. (1971); [(f)]Livingston et al. (1976b).

Table A.4. Computed excitation energies in cm $^{-1}$ for the 45 lowest states in Si IV, as a function of the increasing active set of orbitals, accounting for CV correlation, where n indicates the maximum principle quantum number of the orbitals included in the active set, as well as CC correlation. Observed and computed excitation energies for the Si IV from the NIST-database ($E^a_{\rm obs}$) and the other theoretical study ($E^b_{\rm theor}$) are also given. In the last two columns, the difference ΔE between observed and computed energies is compared for the present and previous studies.

	CV							
Level	n = 10	n = 11	n = 12	CC	$E_{\rm obs}{}^a$	$E^b_{\rm theor}$	$\Delta E_{\rm CC}$	$\Delta E^b_{\rm theor}$
$3s\ ^2S_{1/2}$	0	0	0	0	0	0	0	0
$3p\ ^2P^o_{1/2}$	71407	71353	71351	71211	71288	71159	77	128
$3p\ ^2P^o_{3/2}$	71870	71813	71812	71667	71749	71667	82	81
$3d\ ^2D_{5/2}$	160585	161039	161209	160208	160374	160287	166	87
$3d\ ^2D_{3/2}$	160587	161041	161210	160210	160376	160281	166	94
$4s\ ^2S_{1/2}$	194179	194571	194709	193778	193979	193787	201	192
$4p\ ^2P^o_{1/2}$	218498	218859	218986	218048	218267	218051	219	216
$4p\ ^2P^o_{3/2}$	218661	219020	219147	218208	218429	218234	221	194
$4d\ ^2D_{5/2}$	250200	250743	250933	249767	250008	249827	241	181
$4d\ ^2D_{3/2}$	250200	250743	250933	249768	250008	249821	240	187
$4f\ ^2F^o_{5/2}$	254313	254927	255134	253847	254127	253876	280	251
$4f\ ^2F^o_{7/2}$	254315	254929	255136	253848	254129	253880	281	249
$5s\ ^2S_{1/2}$	265617	266135	266312	265166	265418	265216	252	202
$5p\ ^2P^o_{1/2}$	276718	277218	277387	276244	276504	276281	260	223
$5p\ ^2P^o_{3/2}$	276794	277293	277462	276319	276579	276365	260	214
$5d\ ^2D_{5/2}$	291680	292265	292464	291232	291498	291292	266	206
$5d\ ^2D_{3/2}$	291680	292265	292464	291232	291498	291290	266	208
$5f\ ^2F^o_{5/2}$	293898	294519	294727	293431	293719	293475	288	244
$5f\ ^2F^o_{7/2}$	293899	294520	294728	293432	293719	293477	287	242
$5g\ ^2G_{7/2}$	294007	294638	294847	293549	293838		289	
$5g\ ^2G_{9/2}$	294008	294638	294848	293550	293838		288	
$6s\ ^2S_{1/2}$	299865	300436	300628	299406	299677	299451	271	226
$6p\ ^2P^o_{1/2}$	305839	306398	306585	305365	305641	305405	276	236
$6p\ ^2P^o_{3/2}$	305881	306439	306626	305406	305682	305450	276	232
$6d\ ^2D_{3/2}$	314092	314698	314901	313638	313915	313688	277	227
$6d\ ^2D_{5/2}$	314092	314698	314901	313638	313915	313690	277	225
$6f\ ^2F^o_{5/2}$	315404	316031	316239	314939	315230	314983	291	248
$6f\ ^2F^o_{7/2}$	315404	316031	316240	314940	315230	314983	290	247
$6g\ ^2G_{7/2}$	315475	316106	316315	315016	315305		289	
$6g\ ^2G_{9/2}$	315475	316106	316316	315016	315305		289	
$6h\ ^2H^o_{9/2}$	315482	316118	316327	315023	315317		294	
$6h\ ^2H^o_{11/2}$	315482	316118	316328	315023	315317		294	
$7s\ ^2S_{1/2}$	318924	319520	319719	318463	318743	318505	280	238
$7p\ ^2P^o_{1/2}$	322500	323089	323285	322029	322313	322069	284	244
$7p\ ^2P^o_{3/2}$	322525	323114	323309	322054	322338	322097	284	241
$7d\ ^2D_{3/2}$	327536	328153	328358	327080	327362	327125	282	237
$7d\ ^2D_{5/2}$	327536	328153	328358	327080	327362	327125	282	237
$7f\ ^2F^o_{5/2}$	328370	329001	329210	327908	328200	327950	292	251
$7f\ ^2F^o_{7/2}$	328371	329001	329210	327908	328200	327950	292	250
$7g\ ^2G_{7/2}$	328418	329050	329260	327959	328250		291	
$7g\ ^2G_{9/2}$	328419	329051	329260	327959	328250		291	
$7h\ ^2H^o_{9/2}$	328423	329059	329269	327963	328257		294	
$7h\ ^2H^o_{11/2}$	328423	329059	329269	327964	328257		293	
$7i\ ^2I_{11/2}$	328424	329060	329270	327965	328261		296	
$7i\ ^2I_{13/2}$	328425	329061	329270	327965	328261		296	

References. [(a)]Kramida et al. (2018); [(b)]Froese Fischer et al. (2006).

Table A.5. Results for Si IV: Comparison between computed lifetimes, in length (τ_l) and velocity (τ_v) gauge, from our calculations. These are compared to the predicted lifetimes from other calculations[b,c] ($\tau_{\rm theor}$), as well as experimental results $\tau_{\rm obs}^{d,e}$, with stated uncertainties. All values are given in seconds.

	RCI					
Level	τ_l	τ_v	$\tau_{\rm theor}{}^b$	$\tau_{\rm theor}{}^c$	$\tau_{\rm obs}{}^d$	$\tau_{\rm obs}{}^e$
$3p\ ^2P^o_{1/2}$	1.162E-09	1.159E-09	1.167E-09	1.102E-09		(1.2 ± 0.4)E-09
$3p\ ^2P^o_{3/2}$	1.139E-09	1.138E-09	1.141E-09	1.081E-09		(1.2 ± 0.4)E-09
$3d\ ^2D_{3/2}$	3.923E-10	3.906E-10	3.916E-10	3.790E-10		(4.6 ± 0.5)E-10
$3d\ ^2D_{5/2}$	3.964E-10	3.949E-10	3.962E-10	3.840E-10		(4.6 ± 0.5)E-10
$4s\ ^2S_{1/2}$	2.819E-10	2.827E-10	2.821E-10	2.930E-10		
$4p\ ^2P^o_{1/2}$	9.156E-10	9.150E-10	9.111E-10	9.970E-10		(7.5 ± 0.3)E-10
$4p\ ^2P^o_{3/2}$	9.232E-10	9.221E-10	9.199E-10	9.900E-10		(7.5 ± 0.3)E-10
$4d\ ^2D_{3/2}$	1.808E-09	1.812E-09	1.806E-09	1.824E-09	(2.0 ± 0.2)E-09	(2.1 ± 0.2)E-09
$4d\ ^2D_{5/2}$	1.811E-09	1.816E-09	1.810E-09	1.846E-09	(2.0 ± 0.2)E-09	(2.1 ± 0.2)E-09
$4f\ ^2F^o_{5/2}$	2.638E-10	2.638E-10	2.639E-10	2.620E-10		(4.8 ± 0.4)E-10
$4f\ ^2F^o_{7/2}$	2.638E-10	2.638E-10	2.639E-10	2.620E-10		(4.8 ± 0.4)E-10
$5s\ ^2S_{1/2}$	4.348E-10	4.356E-10	4.322E-10	4.460E-10		
$5p\ ^2P^o_{1/2}$	1.288E-09	1.283E-09	1.269E-09	1.382E-09	(2.1 ± 0.3)E-09	(2.2 ± 0.2)E-09
$5p\ ^2P^o_{3/2}$	1.299E-09	1.293E-09	1.283E-09	1.375E-09	(2.1 ± 0.3)E-09	(2.2 ± 0.2)E-09
$5d\ ^2D_{3/2}$	3.090E-09	3.100E-09	3.058E-09	3.231E-09		
$5d\ ^2D_{5/2}$	3.068E-09	3.078E-09	3.036E-09	3.256E-09		
$5f\ ^2F^o_{5/2}$	4.940E-10	4.934E-10	4.926E-10			
$5f\ ^2F^o_{7/2}$	4.940E-10	4.935E-10	4.927E-10	4.820E-10		
$5g\ ^2G_{7/2}$	9.147E-10	9.154E-10		9.240E-10	(12 ± 2)E-10	(26 ± 3)E-10
$5g\ ^2G_{9/2}$	9.147E-10	9.154E-10		9.240E-10	(12 ± 2)E-10	(26 ± 3)E-10
$6s\ ^2S_{1/2}$	7.062E-10	7.058E-10	6.952E-10	7.160E-10		
$6p\ ^2P^o_{1/2}$	1.957E-09	1.937E-09	1.901E-09	2.063E-09		
$6p\ ^2P^o_{3/2}$	1.975E-09	1.952E-09	1.921E-09	2.056E-09		
$6d\ ^2D_{3/2}$	4.529E-09	4.488E-09	4.376E-09	4.685E-09		
$6d\ ^2D_{5/2}$	4.482E-09	4.445E-09	4.332E-09	4.712E-09		
$6f\ ^2F^o_{5/2}$	8.336E-10	8.289E-10	8.274E-10			
$6f\ ^2F^o_{7/2}$	8.336E-10	8.290E-10	8.274E-10	8.070E-10		
$6g\ ^2G_{7/2}$	1.568E-09	1.569E-09				
$6g\ ^2G_{9/2}$	1.568E-09	1.569E-09		1.569E-09		
$6h\ ^2H^o_{9/2}$	2.373E-09	2.374E-09				(5.2 ± 0.5)E-09
$6h\ ^2H^o_{11/2}$	2.373E-09	2.374E-09		2.376E-09		(5.2 ± 0.5)E-09
$7s\ ^2S_{1/2}$	1.116E-09	1.110E-09	1.077E-09	1.110E-09		
$7p\ ^2P^o_{1/2}$	3.010E-09	2.911E-09	2.808E-09	3.040E-09		
$7p\ ^2P^o_{3/2}$	3.035E-09	2.934E-09	2.837E-09	3.034E-09		
$7d\ ^2D_{3/2}$	6.832E-09	6.366E-09	6.073E-09	6.542E-09		
$7d\ ^2D_{5/2}$	6.732E-09	6.300E-09	6.007E-09	6.553E-09		
$7f\ ^2F^o_{5/2}$	1.325E-09	1.294E-09	1.289E-09			
$7f\ ^2F^o_{7/2}$	1.325E-09	1.294E-09	1.289E-09	1.261E-09		
$7g\ ^2G_{7/2}$	2.473E-09	2.469E-09				
$7g\ ^2G_{9/2}$	2.473E-09	2.470E-09		2.454E-09		
$7h\ ^2H^o_{9/2}$	3.751E-09	3.752E-09				
$7h\ ^2H^o_{11/2}$	3.751E-09	3.753E-09		3.750E-09		
$7i\ ^2I_{11/2}$	5.270E-09	5.272E-09				
$7i\ ^2I_{13/2}$	5.270E-09	5.272E-09		5.267E-09		

Notes. Both the length and velocity forms are displayed for the present RCI calculations. The available lifetimes from experimental measurements and previous calculations are also given.

References. [(a)]Present calculations; [(b)]Froese Fischer et al. (2006); [(c)]Siems et al. (2001); [(d)]Bashkin et al. (1980); [(e)]Berry et al. (1971).